INL/JOU-13-30754
Preprint

COMPUTATIONAL THERMODYNAMIC MODELING OF HOT CORROSION OF ALLLOYS HAYNES 242 AND HASTELLOY^{TM}N FOR MOLTEN SALT SERVICE

Michael Glazoff, Indrajt Charit, Piyush Sabharwall

September 2014

The INL is a
U.S. Department of Energy
National Laboratory
operated by
Battelle Energy Alliance

Prepared for the U.S. Department of Energy
Office of Nuclear Energy
Under DOE Idaho Operations Office
Contract DE-AC07-05ID14517

COMPUTATIONAL THERMODYNAMIC MODELING OF HOT CORROSION OF ALLLOYS *HAYNES 242* AND *HASTELLOY™N* FOR MOLTEN SALT SERVICE

Michael Glazoff[1,*], Indrajt Charit[2], and Piyush Sabharwall[3]

[1]*Advanced Process and Decision Systems Dept., Idaho National Laboratory, Idaho Falls, ID 83415-3710*

e-mail Michael.Glazoff@inl.gov; phone (208) 526 8937 –the author to which all correspondence should be sent

[2]Dept. of Chemical and Materials Engineering, University of Idaho, 875 Perimeter Drive MS3024Moscow, ID 83844-3024

[3]Thermal Science & Safety Analysis Dept., Idaho National Laboratory, Idaho Falls, ID 83415-3730

An evaluation of thermodynamic aspects of hot corrosion of the superalloys Haynes 242 and Hastelloy™ N in the eutectic mixtures of KF and ZrF_4 is carried out for development of Advanced High Temperature Reactor (AHTR). This work models the behavior of several superalloys, potential candidates for the AHTR, using computational thermodynamics tool (ThermoCalc), leading to the development of thermodynamic description of the molten salt eutectic mixtures, and on that basis, mechanistic prediction of hot corrosion. The results from these studies indicated that the principal mechanism of hot corrosion was associated with chromium leaching for all of the superalloys described above. However, Hastelloy™ N displayed the best hot corrosion performance. This was not surprising given it was developed originally to withstand the harsh conditions of molten salt environment. However, the results obtained in this study provided confidence in the employed methods of computational thermodynamics and could be further used for future alloy design efforts. Finally, several potential solutions to mitigate hot corrosion were proposed for further exploration, including coating development and controlled scaling of intermediate compounds in the KF-ZrF_4 system.

I. INTRODUCTION

This study introduces the use of computational thermodynamics to address materials issues pertaining to advanced nuclear reactors. For the last ten years or so, there have been renewed interests in Molten Salt Reactors (MSRs). This interest is justified because of several attractive features of MSRs: (1) Can facilitate actinide burning, (2) Provide fully passive decay heat removal (protection feature), (3) Have higher thermodynamic efficiency, and (4) Facilitate hydrogen production. Current concept such as the Advanced High Temperature Reactor (AHTR) and Fluoride Salt Cooled high temperature reactor (FHR) uses molten salt in combination with solid, stationary fuel. However, much of the MSR-related experience is directly relevant to the AHTR and FHR because of the primary loop reference salt for AHTR and FHR is Li_2BeF_4, which is referred to as "FLiBe," was also used as the primary coolant for MSRs [1]. The motivation of this study was to carry out thermodynamic aspects of hot corrosion of the superalloys Haynes 242 and Hastelloy^{TM} N in the eutectic mixtures of KF and ZrF_4, which is a potential secondary coolant for AHTR.

The issue of hot corrosion of Alloy 242 and Hastelloy-N alloys in molten salt eutectic mixtures is of significant interest and importance in the problems of designing modern modular nuclear reactors such as AHTRs [2,3]; solar energy temporary storage [4]; development of new batteries; corrosion in high-temperature fuel cells such as the molten carbonate and solid oxide fuel cells; functioning of spent nuclear waste processing equipment (e.g., apparatuses Mark-IV and Mark-V at the INL - Fuels Fabrication Complex); etc. [5]. Indeed, the relative compatibility of materials with molten salts, to a significant extent, defines how long equipment might work without experiencing breakdowns or malfunctioning.

Hot corrosion represents a phenomenon of materials degradation when in contact with molten salts and, possibly, aggressive gaseous environment. Most molten salts interact strongly with such environments. In general, this phenomenon has been underappreciated by the nuclear materials community. The problem is exacerbated by the fact that, unlike in aqueous environments with dissolved gases, no Pourbaix diagrams can be constructed for molten salts.[a] Pourbaix diagram highlights the importance of taking into account gaseous environment, which is not very relevant to the conditions at which the secondary coolant loop of molten salt nuclear reactors (AHTRs) function (molten salt is supposed to be hermetically pressurized in the loop piping), it is critically important to elucidate the "molten salt – gaseous phase" interactions for other applications.

Oxidation in hot corrosion can be because of either a component of the gas environment or a salt species. In fact, equivalence could be established between the two from a thermodynamics perspective. In turn, this leads to quite different corrosion processes because of the presence of a thin film of salt compared to the same salt present in secondary coolant loops [6]. Also, the corrosion products (oxides, or fluorides, etc.) are rarely soluble in the salt. Besides, they seldom form any passive films (the importance of Cr_2O_3 stability with respect to aggressive is explored in this report). This means that the product layer is porous, easily subjecting it to further attack by molten salt. Consequently, the formation of different diffusion couples across the thickness of the corrosion product near the metal surface could be expected as concentration of different components changes across the interface [7]. The high temperatures at which molten salts are used also facilitate chemical interactions, leading to increased rates of oxidation [7]. In superalloys where just a couple of components may contribute to the formation of the ultimate corrosion products, diffusion sometimes leads the formation of a depletion zone immediately below the corrosion product layer [8].

---

a What a phase diagram is for a metallurgist, a Pourbaix diagram is for a corrosion scientist. It is plotted in the "pH – E(SHE)" coordinates (electrochemical potential w/r to standard hydrogen electrode vs. pH) and allows constructing areas of stability, passivation, and unchecked corrosion attack for a given electrolyte system.

Another feature typical of molten fluorides is that they can easily dissolve passive oxide layers, while moisture and oxide impurities in fluorides can cause corrosion (oxidation) of the metal alloy. One of the protective measures against these undesirable phenomena is the development of systems for control of coolant chemistry and purification of molten salt materials [4, 6 - 8].

Different methods have been offered to control hot corrosion in AHTR systems: development of advanced, corrosion-resistance alloys; control of redox processes by use of metallic beryllium immersed into the molten salt; control of oxide formation by using high-purity helium as a cover gas; etc. The principal idea is to maintain a reducing (low-oxidation potential) environment in the salt by imposing rigorous REDOX control upon the system [9, 10].

According to previous research, the following materials were assessed as candidates for AHTR designs in different countries: 800H, Alloy N, Hastelloy X, Czech superalloy MONICR (MoNiCr), and a Russian alloy HN80M-VI. The application of many of these materials and silicon carbide (SiC) was explored extensively in a recent Ph.D. thesis at the University of Wisconsin (Advisor–Prof T. Allen) [9]. The chemical compositions of these materials, temperature ranges of their exposure to molten salt mixtures of different chemical compositions, and resistance to molten salt corrosion are described in Table I [11].

Table I. Chemical composition and hot corrosion resistance of the several superalloy materials against hot corrosion [11].

Alloy	Alloy Composition (principal elements) (wt%)	Resistance to Hot Corrosion	Working Temperature Range
Alloy N	Ni base; ~17%Mo; 7% Cr; 5% Fe	Very good	Up to 750°C

Hastelloy X	Ni base; 9% Mo; 20% Cr; 20% Fe	Needs evaluation	Up to 900°C
Alloy 242	Ni - base; ~25% Mo; 8% Cr; 1.5% Fe	Good resistance to high-T fluoride-bearing environments	Up to 815°C
HN80M-VI	Ni - base; 8% Mo; 12% Cr	Very good	High Temperatures
MONICR	Ni - base; 18% Mo; 7% Cr; 2% Fe	Very good	Up to 750°C

Based on the results of this and other research projects, it was decided in this work to explore the hot corrosion stability of Alloy 242 and Alloy N in a molten fluoride mixture of eutectic composition.

While the physical and thermo-physical properties of these materials are known, the issue of hot corrosion, up until recently, has been studied only experimentally [10]. Experimental studies involving molten salts are very difficult, given the aggressive nature of these materials and high temperature of experimentation. Consequently, any modeling efforts aimed at prescreening of candidate materials from the viewpoint of their thermodynamic, diffusion, and corrosion stability, are of interest to the nuclear engineering community.

Such computational thermodynamic and diffusion work has commenced only within the last 10 years or so. Efforts have been made to assess the behavior of generic superalloys in different eutectic[b] molten salt mixtures in order to establish different hot corrosion mechanisms—protection with thin oxide films (typically Cr_2O_3); formation of volatile salts depleting the contents of metals in superalloys; formation of different salts ($CrCl_2$, CrF_2, $CrCl_3$, and CrF_3); and others. While this work is rapidly

[b] Eutectic salt mixtures are used in order to reduce the operating temperatures of different processes. Typically, a working temperature of a given process should be at least 100°C higher than that of the eutectic point to ensure that a highly undesirable solidification would not take place.

developing now in different European research centers in Sweden, Germany, Spain, etc., it is still in its infancy. In part, this situation was caused by the lack of reliable ionic liquid, superalloy, pure substances, and solutions databases and insufficient processing speed of computers. However, the situation has changed dramatically with all of these resources available, allowing for conducting reliable single-point, stepping, and mapping thermodynamic calculations of hot corrosion.

The rest of this section is organized as follows: Section 3.2 gives a brief overview of different molten salts typically used for design of AHTRs; Section 3.3 describes thermodynamic properties and phase equilibria in Alloy 242 and Alloy N; Section 3.4 provides the results obtained in this study and their comparison to existing experimental data, mostly generated at ANL, ORNL, and the University of Wisconsin; and Section 5 provides conclusions and recommendations for future computational and modeling research in this area of nuclear engineering.

I.A. Thermodynamics and Phase Equilibria in Molten Salt Compositions

For the purposes of the present report, only data for the following three candidate salt systems is discussed: NaF-LiF-KF, KCl-$MgCl_2$, and KF-ZrF_4.

I.A.1. NaF-LiF-KF Quasi-Ternary System

Of these three systems, NaF-LiF-KF (also known as FLiNaK) has been studied most extensively. The binary phase diagrams for K-F, Li-F, and Na–F, are presented in Fig. 1.

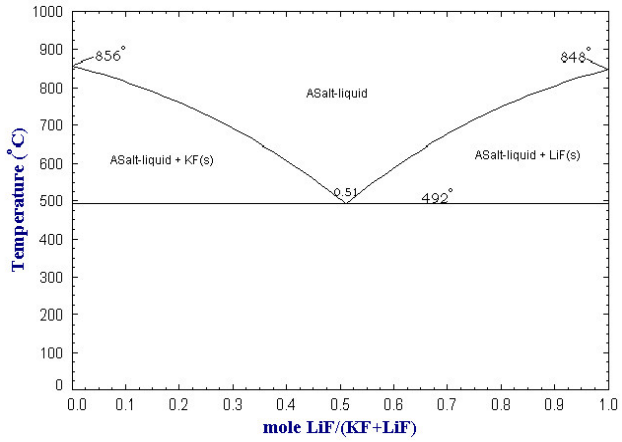

Fig. 1. Phase diagram LiF-KF, after [12].

I.A.1.1. The Quasi-Binary LiF-KF Phase Diagram

Calculations performed using ThermoCalc and the molten salt thermodynamic database, SALT1, yielded the practically identical result shown in Figure 2. The red line(s) represent nonvariant phase transformation lines while tie lines are presented as green lines. While this diagram does not carry any additional information compared to Figure 1, it still illustrates the computational thermodynamics capabilities developed at INL over the last year.

Figure 2 is of a eutectic type characterized by the absence of mutual solubility of either LiF in KF, or of KF in LiF. The temperature of nonvariant eutectic transformation is 492°C at 0.51 mol% of LiF. The liquid phase forming upon melting of these salts is a so-called ionic liquid. As it is typical of molten salts, it is transparent, possesses viscosity similar to that of pure water, and conducts electricity (ionic conductivity). It is this combination of properties that make molten salts so attractive for the applications in different nuclear reactor designs (AHTRs).

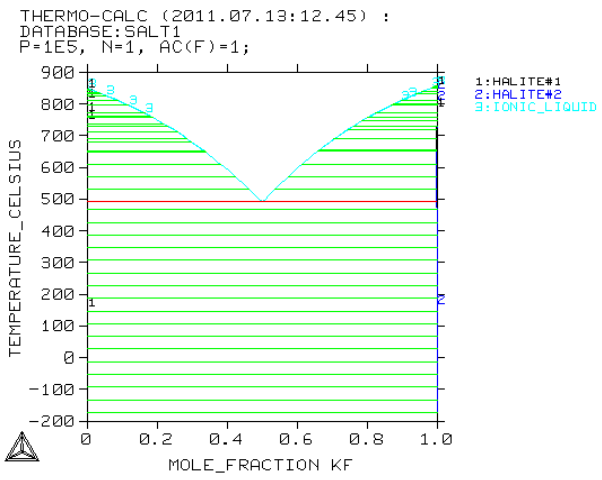

Fig. 2. Quasi-binary phase diagram LiF-KF. While this diagram does not carry any additional information compared to Figure 1, it illustrates the computational thermodynamics capabilities developed at INL during the last year.

I.A.1.2. Quasi-Binary LiF-NaF Phase Diagram

This phase diagram for LiF-NaF is presented in Figure 3 [13].

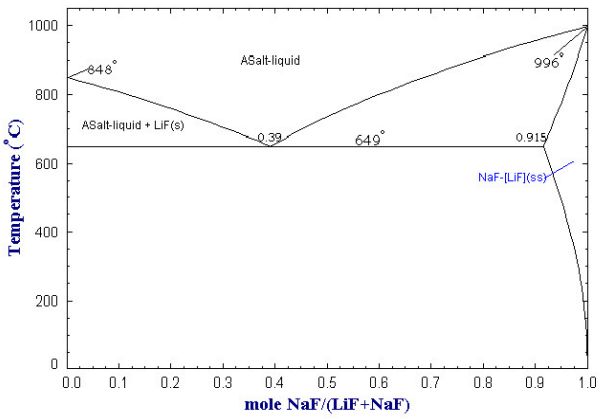

Fig. 3. Phase Diagram NaF-LiF, after [13].

Similar results were obtained in this work using the ThermoCalc software as shown in Figure 4.

As can be seen from Figure 3 and Figure 4, there is some solubility of LiF in NaF, but no solubility of NaF in pure LiF. The nonvariant eutectic transformation takes place at 649°C, with the eutectic point being at 0.39 mol % NaF.

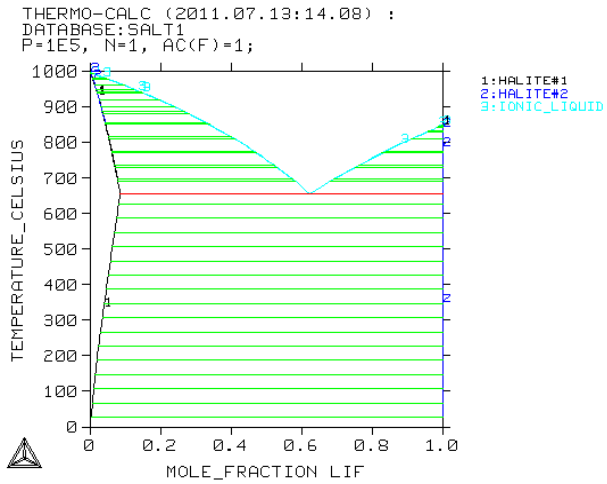

Fig. 4. ThermoCalc calculations in the present work, NaF-LiF phase diagram. Halites 1 and 2 correspond to solid LiF and NaF, respectively. Also see note to Fig. 2 above.

I.A.1.3. Quasi-Binary KF-NaF Phase Diagram

The KF-NaF phase diagram is given in Fig. 5.

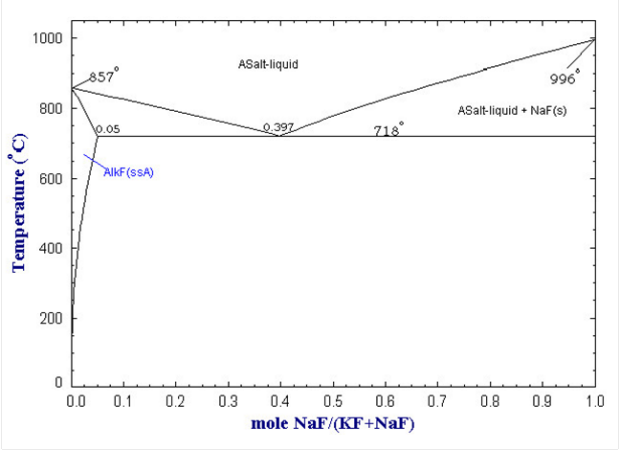

Fig. 5. The NaF-KF phase diagram, after [13].

ThermoCalc calculations yielded very similar results as shown in Fig. 6.

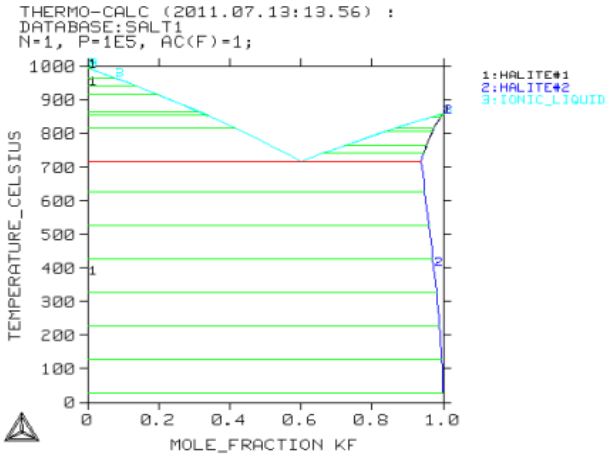

Fig. 6. ThermoCalc calculations of the NaF-KF phase diagram.

The eutectic temperature is at 718°C; and the eutectic point corresponds to the 0.397 molar fraction of NaF. Of the three binary diagrams, the eutectic temperature is the highest for the NaF-KF phase.

Consequently, the need arises to use a three-component system in which the ternary eutectic temperature will lie lower than in the binary systems considered above.

I.A.1.4. Ternary Phase Diagram LiF-KF-NaF

The ternary diagram for LiF-KF-NaF presented in Fig. 7 [11] clearly demonstrates the advantage of a ternary system over the corresponding binaries; the ternary eutectic point temperature falls to 457°C, while the lowest binary eutectic temperature is 492°C (for the KF-LiF system).

The ternary KF-LiF-NaF system is not assessed in the SALT1 database, so the law of ideal solutions extrapolating from these binaries to the ternary system was tried. Unfortunately, the resulting eutectic point temperature was T_e=491°C, nearly the value coinciding with that of the binary KF-LiF eutectic. Future work on the database development will need to be undertaken for this and other systems of interest.

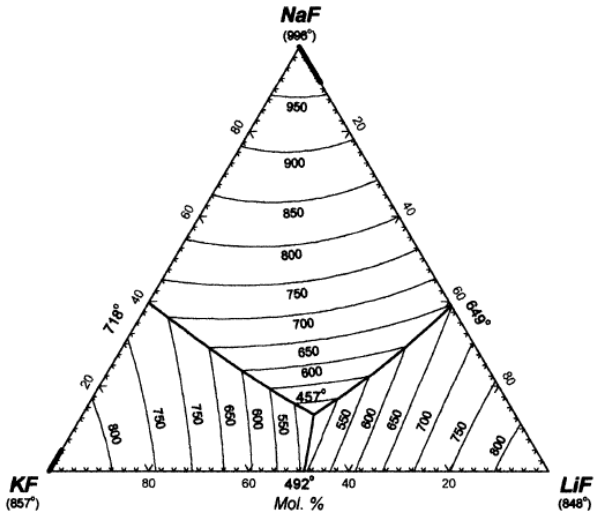

Fig. 7. Polythermal (liquidus) projection diagram for the LiF-NaF-KF ternary system [12].

I.A.2. Eutectic KCl –$MgCl_2$ Binary System

The phase diagram for the KCl-$MgCl_2$ system is presented in Figure 8 [13]. The FTSalt database belonging to FactSage was used in these calculations.

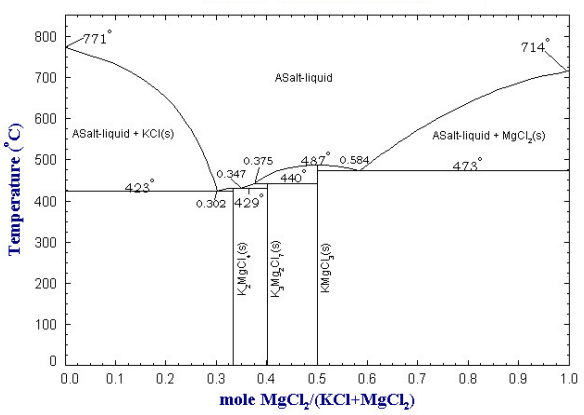

Fig. 8. Phase diagram of the KCl – $MgCl_2$ system [13].

As can be seen in this phase diagram, it is characterized by the practically nonexistent solubility of both species (KCl and $MgCl_2$) in each other. Also note the formation of three distinctive compounds: K_2MgCl_4 (forms at 429°C according to peritectic reaction), $K_3Mn_2Cl_7$ (forms according to peritectic reaction at 440°C), and $KMgCl_3$ (melts congruently at 487°C). Typically, to avoid solidification, the working temperature is kept at least 100°C above the onset of solidification. According to Sabharwall et al. [2], the concentration point for this system was chosen at 68 mol% KCl and 32 mol% $MgCl_2$. This is very close to the deep eutectic point (423°C; 0.302 mol% $MgCl_2$). The inlet and outlet temperatures in the reactor design [2] are going to be 679°C and 587°C, respectively. The choice of chemical

composition is excellent, resulting in a safety cushion of at least 150°C above the liquidus line for this composition.

I.A.3. Phase Diagram KF-ZrF_4.

This quasi-binary system is the least studied for AHTR molten salt applications. The corresponding phase diagram was not found in available open literature, and it could not be assessed thermodynamically because of the lack of data in the SALT1 database by ThermoCalc or FSalt database by FactSage. The work on expanding this thermodynamic database to include the assessed KF-ZrF_4 phase diagram has commenced at INL.

I.B. Chemical Compositions and Microstructure of Alloy 242 and Alloy N

I.B.1. Alloy 242

This alloy was developed more than 40 years ago, and its properties, microstructure, and behavior in oxidizing environments have been studied quite extensively [15, 16]. To understand its phase composition as a function of temperature and pressure, typically quasi-binary diagrams (property diagrams) are constructed [14, 17]. Such diagrams can be studied currently using well-regressed thermodynamic databases and fast, efficient algorithms of the global Gibbs energy minimization to establish equilibrium conditions.

In order to probe this alloy's microstructure at temperatures from 600 to ~720°C, we have constructed the carbon isopleth for Alloy 242 as shown in Figure 10. As can be seen in Figure 9, this is

an austenitic matrix alloy with particles of Ni_2Me and, depending upon its heat treatment, μ-phase, δ–phase, and γ'-precipitates.

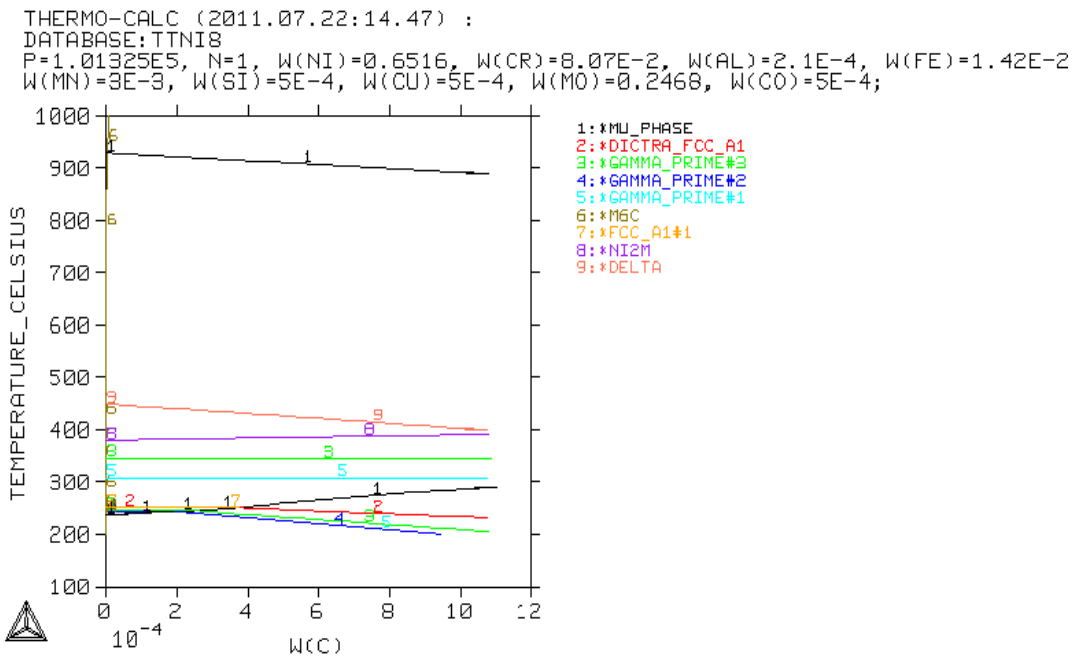

Fig. 10. Carbon isopleth for Haynes-242.

A microstructural characterization of a Alloy 242 nickel-molybdenum-chromium superalloy was performed [2]. Molybdenum was found to partition to the lenticular $Ni_2(Mo,Cr)$ precipitates, whereas iron, aluminum, silicon, manganese and nickel were found to partition to the γ matrix. Chromium was not found to partition significantly between the phases. Atom probe tomography and energy-filtered transmission electron microscopy core-loss images revealed boron, molybdenum, chromium, phosphorus, and carbon segregation to the grain boundaries. Despite the size of the precipitates being larger after a two-step heat treatment of 16 hours at 704°C plus 16 hours at 650°C compared to a one-step heat treatment of 48 hours at 650°C, no significant differences were found in the mechanical properties or compositions of the phases.

The formation of the Ni_2M intermetallic phase takes place at somewhat lower temperatures, around 400°C, as shown in Figure 10. However, overall, this is a reasonable set of phases to be expected for Alloy 242 at this temperature range, because the alloy's ultimate microstructure and phase composition will be determined by the heat treatments used during its thermo-mechanical processing.

I.B.2. Alloy N

Alloy N is a nickel-based alloy invented at Oak Ridge National Laboratories as a container material for molten fluoride salts. Its hot corrosion mechanism has been studied extensively and reported by McKoy, Jr. [18]. It has good oxidation resistance to hot fluoride salts in the temperature range of 1300 to 1600°F (704 to 871°C).

The carbon isopleth (property diagram) of this alloy was constructed similar to Figure 10. Figure 11 shows that the equilibrium phases for this alloy are carbide M_6C, γ' strengthening precipitates, and μ–phase. This is similar to Alloy 242, but no Ni_2M formation is expected in this case.

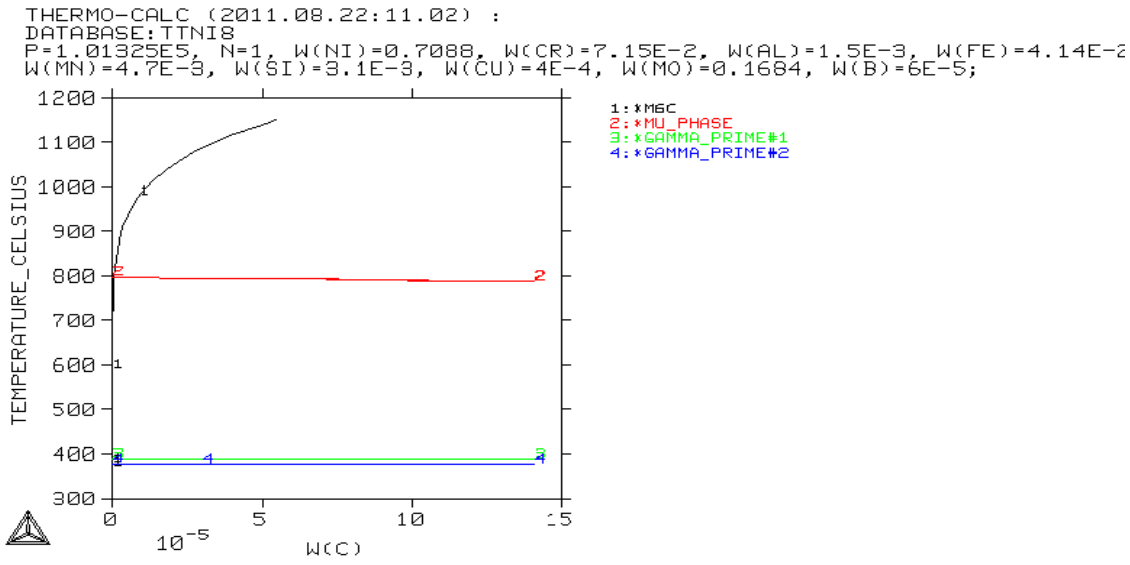

Fig. 11. Carbon isopleth (property diagram) for Hastelloy-N.

I.C. Modeling of Corrosion Behavior of Haynes-242 and Hastelloy-N in Molten Salt Environment

As indicated in the introduction to Section 3, the specifics of hot corrosion are in the dissolution of protective oxides that might be formed on the metal surface. It is also very important to realize that the composition of molten salt mixture will strongly depend on the composition of the gaseous phase. Consequently, all of these factors need to be taken into account when modeling hot corrosion phenomena.

Perhaps the most detailed study of hot corrosion of different materials, including Alloy N and SiC, was given in a recent experimental work by Olson [10]. This researcher studied a mixture of LiF-NaF-KF (46.5–11.5-42 mol% (commonly referred to as FLiNaK), as well as a molten chloride near eutectic salt, KCl-$MgCl_2$: 6832 mol%. The following high-temperature alloys and materials have been studied in these molten salt environments: Hastelloy-N, Hastelloy-X, Haynes-230, Inconel-617, and Incoloy-800H, Nb-1Zr, a nearly pure nickel alloy Ni-201, and a C/Si SiC ceramic. After exposure to molten FLiNaK at 850°C for 500 hours in sealed graphite crucibles under argon cover gas corrosion was established to occur predominantly from de-alloying of chromium from the chromium bearing alloys, an effect that was particularly pronounced at the grain boundaries.

Similar conclusions were made by Koger and Litman [19], who studied compatibility of Hastelloy-N and Haynes Alloy No. 25 in a molten sodium fluoroborate mixture. It was determined in the range from 460 to 605°C. The cobalt-base alloy (Haynes 25) was inadvertently incorporated in the Alloy N thermal convection loop and was exposed to the fluoroborate salt mixture for 3,660 hours. The Haynes 25 alloy suffered damage by selective leaching of cobalt and chromium, which migrated to the Alloy N. The

mechanism of corrosive attack was activity gradient and temperature-gradient mass transfer. Haynes 25 alloy is more susceptible to attack by the fluoroborate mixture than Alloy N.

Consequently, special attention has been paid to the issues of chromium leaching from these two alloys, the formation of Cr_2O_3 on the surface, which in some cases has been shown to serve as a protective barrier against further hot corrosion attack, and its dissolution under certain harsh environmental conditions.

It is important to note that, in all of these calculations, oxygen was supposed to be directly present in the gaseous phase (not suspended or rejected phase).

I.C.1 General Considerations on the Stability of Protective Oxide Cr_2O_3 on Alloy 242 and Alloy N Surfaces

It is an established fact that, in many cases, further oxidation of stainless steel and/or superalloy surfaces can be arrested if Cr_2O_3 is formed on the surface. This is also true of other oxides such as Al_2O_3. However, under extremely aggressive conditions, the Cr_2O_3 layer may be dissolved by the attacking salts, or gases, resulting in an alloy becoming prone to corrosion attacks from oxidizing environments.

In the computational thermodynamics literature [20], an example was considered elucidating the behavior of Cr_2O_3 in the presence of an aggressive environment comprised of such elements as carbon, hydrogen, nitrogen, oxygen, sulfur, and the molten salt, NaCl. While the exact chemical composition of the gaseous phase will be defined by the conditions of chemical and phase equilibria, it could be hypothesized that it could be comprised of hydrogen H_2; SO_2; nitrogen N_2 (from the air); and CO. Such

a mixture could represent a contaminated syngas, and the process would then model its interaction with the steel or superalloy surfaces [20].

These calculations have been repeated in this work for the temperature range from 200 to 1300°C, and ambient pressure. The results are presented in Figures 12 and 13.

In Figure 12, the solid green line corresponds to Cr_2O_3; the red line to NaCl (melting begins at around 730°C). Other phases present are the gaseous phase (black line); halite (5, light blue), orthorhombic (6, dark green) and hexagonal (4, dark brown). It can be seen that chromia remains stable in this very aggressive atmosphere and molten salt up to ~1,000°C. Beyond this temperature, a rapid Cr_2O_3 dissolution process takes place.

Figure 13 shows how chromium is distributed among the several thermodynamically stable phases in the system. It shows a growing concentration of chromium-bearing compounds in the gaseous phases (1, black); and the onset of chromium concentration increase in ionic liquid (2, red) beginning at ~1000°C [20].

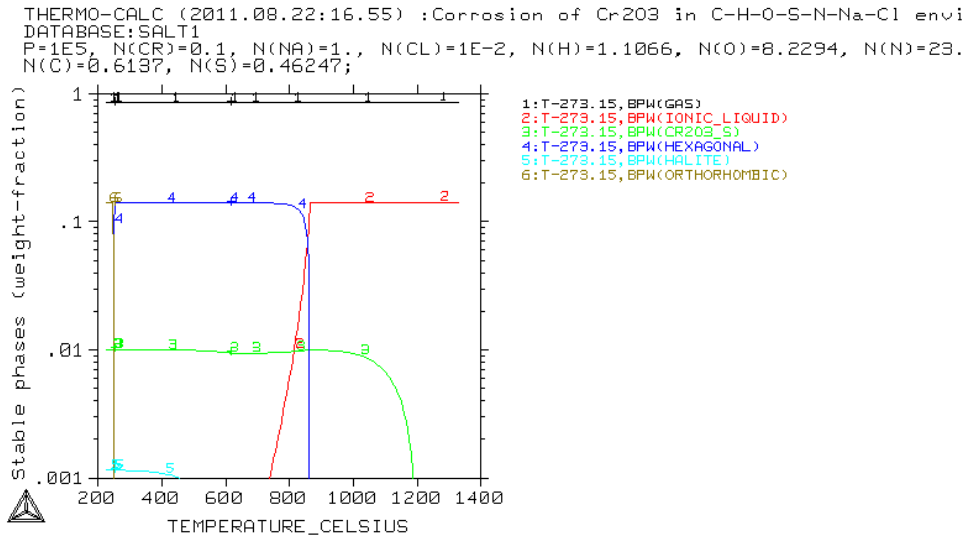

Fig. 12. Stable phases in the Cr_2O_3 – molten salt NaCl – C - H –O –N –S system [20]

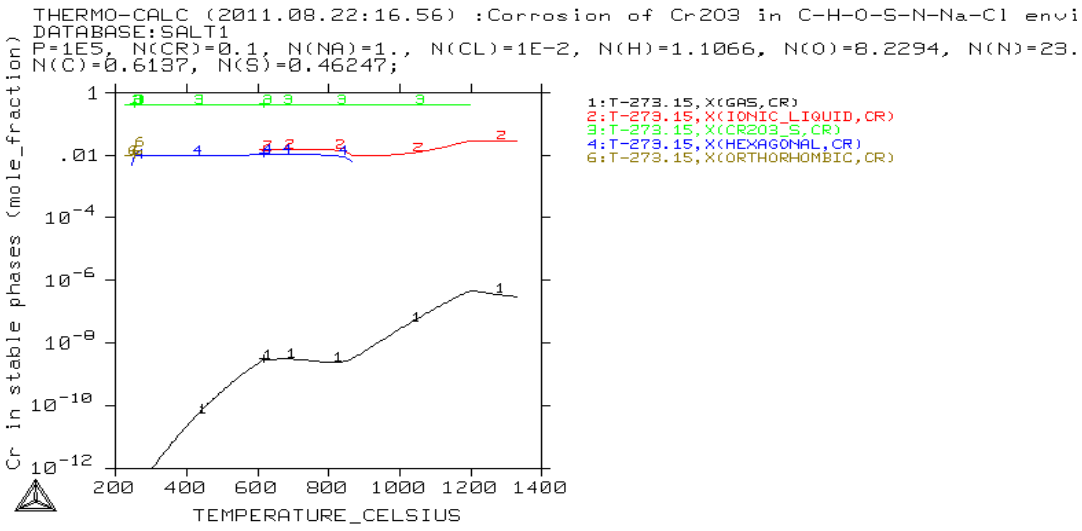

Fig. 13. Distribution of chromium in stable phases as a function of temperature [20]

Overall, these data support the fact that Cr_2O_3 could provide a high degree of protection of chromium-bearing Alloy 242 and Alloy N, provided it is deposited upon the surface in a compact in a contiguous way. This conclusion will need to be further evaluated experimentally.

Figure 14 illustrates the formation of a protective layer of Cr_2O_3 in a generic stainless steel Fe-chromium submerged into a eutectic mixture of molten salts KCl and $ZnCl_2$ [18]. It also gives an idea of what modeling techniques are used by the computational thermodynamics community for analysis of hot corrosion phenomena in molten salts.

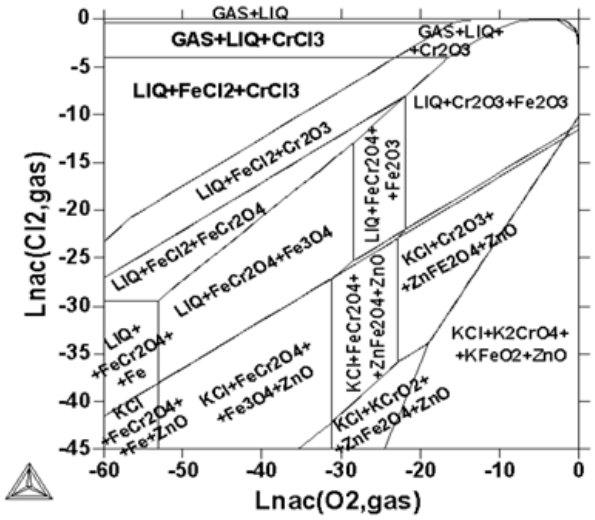

Fig. 14. The representation of the "iron-chromium" generic stainless steel in eutectic mixture of salts KCl and $MgCl_2$ [20]

I.C.2 Construction of a Simplified Thermodynamic Model for the KF-ZrF_4Molten Salt

In general, a self-consistent assessment of thermodynamic data and phase equilibria represents a complex optimization problem. [14, 17, 21-25]. The key requirement to successful optimization and assessment is sufficient amount of data on thermodynamic properties of components, intermediate phases, solid solutions, and the liquid phase.

In a recent research effort by Benes [26], this general approach was used for the assessment of 32 molten salt systems. Unlike in this study, the FactSage computational platform was used for conducting the corresponding thermodynamic assessments. Unlike ThermoCalc Classic version S used in this study, FactSage possesses a very convenient Windows interface that makes access to thermo-chemical data straightforward. However, ThermoCalc can be used together with diffusion

and microstructure evolution modeling software, DICTRA and MICRESS, correspondingly. Also, it provides an opportunity for a seamless coupling with CFD codes such as ASPEN.

Taking into account the time constrains associated with this study, a conclusion was made to pursue a simpler path rather than a full-scale phase-diagram assessment at this time. Indeed, the experimental phase equilibria data found, relates only to the temperatures of melting of the both compounds and to the temperatures and compositions corresponding to the six invariant phase reactions in this system. Any experimental data on phase equilibria in the solid state is practically absent; in the liquid phase. Data on the liquidus temperatures is available but limited.

Available thermodynamic data is also scarce and there are only two publications available on this subject, [27, 28]. Free energies of formation, heat capacities, and their thermal dependencies for the KF and ZrF_4 terminal compounds (the public domain thermodynamic database for pure substances SSUB4 was used for that purpose) were established. The free energies of formation of a number of intermediate compounds in this system were also calculated, using simple rules of thermochemistry. However, these are not experimental values, and any information on the temperature dependence of heat capacity in the solid state is absent. There is just one experimental point for heat capacity in the liquid phase—at the composition corresponding to the deep eutectic in this system, C_p = 1051 J/kg K [3], which is assumed to be independent of temperature.

One could use the sketch phase diagram given in [29, 30] in such a situation, then use an appropriate digitizing and convert at least some portions of the liquidus curve into experimental data. Then, using these experimental points and calculated values of the free energies for all compounds, try to use the optimization module called PARROT (a part of the Thermo-Calc software [25]) to achieve a reasonable agreement between experiment and calculations. However, even assuming the simplest possible variant (complete absence of solubility on the basis of all individual compounds,

their ideal behavior in the solid phase, and an ideal solution model in the liquid phase described in the thermo-chemical module of the Thermo-Calc called GIBBS) it would inevitably end up trying to solve inverse ill-posed problems of experimental data reconstruction. In this case, one would be trying to use the experimental phase diagram to obtain information on the thermodynamic properties of the mixtures.

An excellent example was given by Lukas, Fries, and Sundman [17] who considered a hypothetical situation of assessing a binary system A-B in the absence of any thermodynamic data. They demonstrated that using the thermodynamic models with and without ordering in the solid phase, the phase diagrams were remarkably similar; but a very significant difference was observed in the predicted thermodynamic properties of materials [17].

However, in the present case, with the exception of pure KF and ZrF_4, even experimental data on phase equilibria in the KF-ZrF_4 system is missing, not to mention any thermodynamic results. This situation makes any self-consistent assessment effort hardly feasible at this time.

This situation therefore calls for a different, albeit simplified approach that at least provides some guidance in terms of the possible outcomes of hot corrosion of Hastelloy^{TM} N and Haynes 242. Using the public domain database for pure substances, SSUB4, thermo-chemical data for both KF and ZrF_4 were extracted. In order to construct a thermodynamic model of the liquid phase, the approximation of ideal solutions was used, without any adjustable parameters. Finally, a liquid solution was obtained corresponding to the eutectic point as determined from the corresponding simple eutectic phase diagram constructed on the basis of this model. All subsequent extractions were carried with this model of the liquid phase. The corresponding phase diagram is given in Figure 24 below:

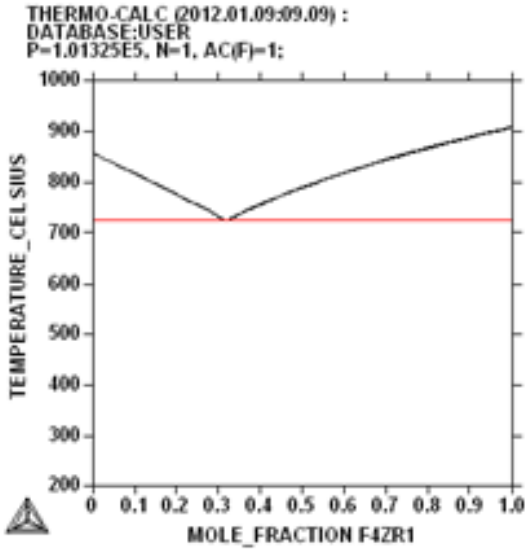

Fig.15. Phase diagram KF-ZrF_4 constructed under the assumption of the ideal behavior of liquid phase [32]

The results of work of the Thermo-Calc script (computation of ZrF_4-KF phase diagram) are presented in Appendix 3. It is very important to understand the limitations of the adopted approach. In turn, to achieve this goal, one needs to have a clear idea of the assumptions that were made in this process. These assumptions are as follows:

- A full assessment of the phase diagram was not performed with all four of its intermediate compounds.
- It was assumed that there is no solubility of solid KF in all three of the polytypes of ZrF_4 in solid KF, and that there is no solubility of solid polytypes of ZrF_4 in solid KF.
- It was assumed that any mixture of molten salts KF and ZrF_4 can be described using the ideal solution model.

This corresponds, in fact, to assuming that a simple eutectic diagram (without any intermediate compounds) would be satisfactory to predict the behavior of a eutectic molten salt composition and to use it in all subsequent work on hot corrosion of superalloys.

How reasonable are these assumptions? As far as mutual solubility of KF and ZrF_4 is concerned, one can be quite confident that neglecting it is reasonable because of the different crystalline structure of KF and ZrF_4 (rock salt cubic for KF versus tetragonal or monoclinic for ZrF_4). Using the well-established Richardson extrapolation procedure also does not raise any serious suspicion because the thermodynamic data for the pure substances (and the errors of their measurement) are very well established. Perhaps the most serious reason for concern is omitting all of the four intermediate compounds from calculations. Indeed, one would probably need to use some variant of the sublattice model [17] with ordering to adequately describe these complex phases in the solid state. Furthermore, the existing Raman spectroscopy data leave no doubt about the existence of short-range ordering in the liquid phase and the existence of complex anions (e.g., ZrF_6^{2-} and $Zr_2F_{10}^{2-}$ coordinated with cations of K^+), [32]. In our calculations, we had to neglect these effects. Still, the behavior of strongly associated molten salt mixtures with significant negative deviations from ideality is much better represented by the ionic liquid model. Nevertheless, in the absence of more detailed information on thermodynamic properties and phase equilibria, there is no choice but to adopt this simplified approach, which is justified because experimental work with molten salts is very costly and requires special equipment and training. Some of the hot corrosion work is planned to proceed at the University of Wisconsin later in 2012/2013. This work will allow comparing the results of predictions made in the present computational study, to valuable experimental information.

I.C.3. Hot Corrosion of Nickel-Based High-temperature Alloys (Alloy 242 and Alloy N in FLiNaK)

The problem of the quantitative assessment of hot corrosion for such complex multicomponent alloys as Alloy 242 or Alloy N is extremely complicated from the computational thermodynamics perspective. The need to work with at least three data bases (TTNI8, SALT1, and SSUB4 (for superalloys, molten salts–ionic liquids, and pure substances) rapidly makes the overall number of competing phases astronomical. In such a situation, even a high-quality global equilibrium solver may yield unphysical results. To make this problem more tractable, the researcher needs to reduce the number of components in the system without jeopardizing the quality of the results, making reasonable assumptions about phases that might be formed at conditions of interest and a realistic representation of the initial set of phases in the system.

After tedious computer experimentation, it was decided to reduce Alloy 242 and Alloy N to Poor Man's 242 and Poor Man's N," respectively. More specifically, it was assumed that the behavior of multicomponent Alloy 242 can be realistically described using just four components: molybdenum, iron, chromium, and the balance going to nickel. In such a formulation, the composition of Alloy N, in wt%, is given as follows: Ch-7.2%; Mo-16.8%; Fe- ~0.5%, and the balance-nickel. For Alloy 242 proceeding in a similar fashion, we get Ch-8.1%; Mo-24.7%; Fe-1.4%; and the balance-nickel (65.2%).

Since the ternary system KF-LiF-NaF was not assessed in database SALT1, the binary system KF-LiF was used. This assumption seems to be reasonable because the introduction of the third salt, NaF, reduces the temperature of eutectic to ~457°C, while for the binary system KF-LiF it was assessed as 492°C. No qualitative changes were expected in the behavior of the whole system as there are not ternary intermediate compounds, or binary compounds in the corresponding phase diagrams.

A simple ThermoCalc script was prepared to model the hot corrosion process at ~600°C, which is given in Figure 16. As can be seen from the script, all calculations were made for 1 mole of the "Alloy N + molten salt" mixture, and at ambient pressure.

```
@@ Modeling the process of hot corrosion in alloy N
go data
swi ttni8
def_sys ni cr mo fe k li f
lis-sys p
get
app
salt1
def_sys ni cr mo fe li k f
get
app
ssub4
def_sys fe cr mo ni li k f
lis-sys p
rej pha *
res pha gas:g cr1f2_s cr1f2_l cr1f3_s cr1f3_l cr1f4_s
res pha f2fe1_s f2fe1_l f2Ni1_s f2ni1_l f3fe1_s
f2fe1_l
res pha f3mo1_s f5mo1_s f5Mo1_l f6mo1_l
res pha f2ni1_s f3ni1_s
lis-sys p
get
go pol
s-c n=1 p=1e5 t=873.15
s-c x(ni)=.375136
s-c x(cr)=.047713
s-c x(mo)=.054939
@@ We expect to work only with ionic liquid, so it
is not necessary to
@@ go to the Gibbs-module of ThermoCalc to
define compounds LiF and KF,
@@ as it was necessary when constructing binary
phase diagrams
s-c x(li)=.1225
s-c x(K)=.1225
```

Fig. 16. ThermoCalc script for assessing hot corrosion of Alloy N in FLiNaK approximated by a binary mixture LiF–KF.

The results shown in Figure 17 were obtained from a so-called "single point" equilibrium calculation. These results provide a very reasonable equilibrium picture for both alloys—FCC-matrix, and a small amount of the μ-phase. There is also an ionic liquid phase and an infinitely small amount of solid CrF_2 (this is denoted with blue oval in Figure 17). This latter result is very important because it demonstrates how the process of corrosion of Alloy N could begin by leaching chromium from the alloy's composition.

The next step was to assess how the hot corrosion process might develop if the chemical activity of fluoride varies, so that the severity of hot corrosion attack could be compared for Alloy 242 and Alloy N. This was done by varying the chemical activity of F. However, since it was assumed that there is practically no F_2 in the gaseous phase, the status of the F_2 gas was set to "suspended" or "dormant" (in the latter case only the driving forces would be computed for this phase, but its amount is assumed to be zero).

Proceeding in a way similar to the oxidation of these two alloys, the following results were obtained. First, conducting a single-point calculation for pure molten salt mixture, the expected results were confirmed after the modeling of oxidizing of Alloy 242 and Alloy N; Alloy 242 is more prone to hot corrosion than Alloy N. This is illustrated by Figure 17.

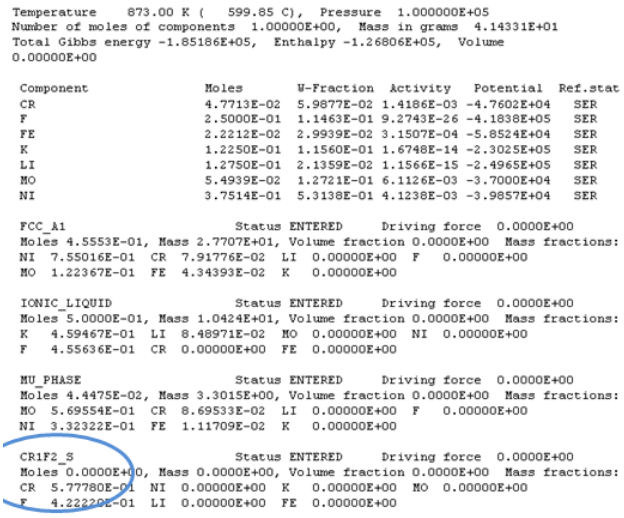

```
Temperature    873.00 K (   599.85 C),  Pressure  1.000000E+05
Number of moles of components  1.00000E+00,  Mass in grams  4.14331E+01
Total Gibbs energy -1.85186E+05,  Enthalpy -1.26806E+05,  Volume
0.00000E+00

 Component               Moles       W-Fraction  Activity   Potential  Ref.stat
 CR                      4.7713E-02  5.9877E-02 1.4186E-03 -4.7602E+04   SER
 F                       2.5000E-01  1.1463E-01 9.2743E-26 -4.1838E+05   SER
 FE                      2.2212E-02  2.9939E-02 3.1507E-04 -5.8524E+04   SER
 K                       1.2250E-01  1.1560E-01 1.6748E-14 -2.3025E+05   SER
 LI                      1.2750E-01  2.1359E-02 1.1566E-15 -2.4965E+05   SER
 MO                      5.4939E-02  1.2721E-01 6.1126E-03 -3.7000E+04   SER
 NI                      3.7514E-01  5.3138E-01 4.1238E-03 -3.9857E+04   SER

 FCC_A1                        Status ENTERED     Driving force  0.0000E+00
 Moles 4.5553E-01, Mass 2.7707E+01, Volume fraction 0.0000E+00  Mass fractions:
 NI  7.55016E-01  CR  7.91776E-02  LI  0.00000E+00  F   0.00000E+00
 MO  1.22367E-01  FE  4.34393E-02  K   0.00000E+00

 IONIC_LIQUID                  Status ENTERED     Driving force  0.0000E+00
 Moles 5.0000E-01, Mass 1.0424E+01, Volume fraction 0.0000E+00  Mass fractions:
 K   4.59467E-01  LI  8.48971E-02  MO  0.00000E+00  NI  0.00000E+00
 F   4.55636E-01  CR  0.00000E+00  FE  0.00000E+00

 MU_PHASE                      Status ENTERED     Driving force  0.0000E+00
 Moles 4.4475E-02, Mass 3.3015E+00, Volume fraction 0.0000E+00  Mass fractions:
 MO  5.69554E-01  CR  8.69533E-02  LI  0.00000E+00  F   0.00000E+00
 NI  3.32322E-01  FE  1.11709E-02  K   0.00000E+00

 CR1F2_S                       Status ENTERED     Driving force  0.0000E+00
 Moles 0.0000E+00, Mass 0.0000E+00, Volume fraction 0.0000E+00  Mass fractions:
 CR  5.77780E-01  NI  0.00000E+00  K   0.00000E+00  MO  0.00000E+00
 F   4.22220E-01  LI  0.00000E+00  FE  0.00000E+00
```

Fig. 17. The results of a single-point calculation for T=600°C, Alloy N.

```
Conditions:
 N=1, P=1E5, T=873, X(NI)=0.349, X(CR)=5.79E-2, X(MO)=8.57E-2, X(LI)=0.1225,
    X(K)=0.1225, X(F)=0.25
 DEGREES OF FREEDOM 0

 Temperature    873.00 K (   599.85 C),  Pressure  1.000000E+05
 Number of moles of components  1.00000E+00,  Mass in grams  4.27974E+01
 Total Gibbs energy -1.83933E+05,  Enthalpy -1.25928E+05,  Volume  0.00000E+00

 Component               Moles       W-Fraction  Activity   Potential  Ref.stat
 CR                      5.7900E-02  7.0345E-02 1.6069E-03 -4.6697E+04 SER
 F                       2.5000E-01  1.1098E-01 8.7139E-26 -4.1884E+05 SER
 FE                      1.2400E-02  1.6181E-02 2.1073E-04 -6.1443E+04 SER
 K                       1.2250E-01  1.1191E-01 1.8605E-14 -2.2948E+05 SER
 LI                      1.2250E-01  1.9867E-02 1.1804E-15 -2.4950E+05 SER
 MO                      8.5700E-02  1.9212E-01 5.9114E-03 -3.7243E+04 SER
 NI                      3.4900E-01  4.7860E-01 4.1545E-03 -3.9803E+04 SER

 FCC_A1                        Status ENTERED     Driving force  0.0000E+00
 Moles 3.7715E-01, Mass 2.3011E+01, Volume fraction 0.0000E+00  Mass fractions:
 NI  7.55741E-01  CR  8.66149E-02  LI  0.00000E+00  F   0.00000E+00
 MO  1.30299E-01  FE  2.73447E-02  K   0.00000E+00

 IONIC_LIQUID                  Status ENTERED     Driving force  0.0000E+00
 Moles 4.9000E-01, Mass 1.0294E+01, Volume fraction 0.0000E+00  Mass fractions:
 K   4.65256E-01  LI  8.25955E-02  MO  0.00000E+00  NI  0.00000E+00
 F   4.52149E-01  CR  0.00000E+00  FE  0.00000E+00

 MU_PHASE                      Status ENTERED     Driving force  0.0000E+00
 Moles 1.2535E-01, Mass 9.2673E+00, Volume fraction 0.0000E+00  Mass fractions:
 MO  5.63679E-01  CR  9.57684E-02  LI  0.00000E+00  F   0.00000E+00
 NI  3.33724E-01  FE  6.82870E-03  K   0.00000E+00

 CR1F2_S                       Status ENTERED     Driving force  0.0000E+00
 Moles 7.5000E-03, Mass 2.2498E-01, Volume fraction 0.0000E+00  Mass fractions:
 CR  5.77780E-01  NI  0.00000E+00  K   0.00000E+00  MO  0.00000E+00
 F   4.22220E-01  LI  0.00000E+00  FE  0.00000E+00
```

Fig. 18. The results of a single-point calculation for T=600°C, Alloy 242.

This conclusion is reached because, under similar conditions, Alloy 242 forms more CrF_2 than Alloy N—finite, albeit a very small amount (0.7E-3 moles) vs. an infinitesimally small amount of CrF_2 for Alloy N.

For Alloy N, in “mild” and “aggressive” conditions (corresponding to increasing chemical activity of F), the results are illustrated by Figures 19 and 20.

```
Conditions:
N=1, P=1E5, T=873, X(NI)=0.375136, X(CR)=4.7713E-2, X(MO)=5.4939E-2,
   X(LI)=0.1225, X(K)=0.1225, LNACR(F)=-49
DEGREES OF FREEDOM 0

Temperature    873.00 K (   599.85 C),  Pressure  1.000000E+05
Number of moles of components  1.00000E+00,  Mass in grams  3.78650E+01
Total Gibbs energy -2.17432E+05,  Enthalpy -1.60979E+05,  Volume  0.00000E+00

Component              Moles       W-Fraction  Activity   Potential  Ref.stat
CR                     4.7713E-02  6.5519E-02 4.4390E-11 -1.7303E+05 SER
F                      3.4043E-01  1.7081E-01 5.2429E-22 -3.5567E+05 GAS
FE                     3.6686E-13  5.4108E-13 0.000E+000 -1.2507E+15 SER
K                      1.2250E-01  1.2649E-01 3.0922E-18 -2.9265E+05 SER
LI                     1.2250E-01  2.2455E-02 1.9619E-19 -3.1266E+05 SER
MO                     4.6864E-02  1.1874E-01 1.2895E-03 -4.8295E+04 SER
NI                     3.2000E-01  4.9599E-01 7.9677E-03 -3.5076E+04 SER

FCC_A1                       Status ENTERED     Driving force  0.0000E+00
Moles 3.6686E-01, Mass 2.3277E+01, Volume fraction 0.0000E+00  Mass fractions:
NI  8.06841E-01  CR  1.61963E-08  LI  0.00000E+00  F   0.00000E+00
MO  1.93159E-01  FE  8.80195E-13  K   0.00000E+00

IONIC_LIQUID                 Status ENTERED     Driving force  0.0000E+00
Moles 4.9000E-01, Mass 1.0294E+01, Volume fraction 0.0000E+00  Mass fractions:
K   4.65256E-01  LI  8.25955E-02  MO  0.00000E+00  NI  0.00000E+00
F   4.52149E-01  CR  0.00000E+00  FE  0.00000E+00

CR1F2_S                      Status ENTERED     Driving force  0.0000E+00
Moles 1.4314E-01, Mass 4.2938E+00, Volume fraction 0.0000E+00  Mass fractions:
CR  5.77780E-01  NI  0.00000E+00  K   0.00000E+00  MO  0.00000E+00
F   4.22220E-01  LI  0.00000E+00  FE  0.00000E+00
```

Fig. 19. Hot corrosion of Alloy N under “mild” conditions, ln[ac(F)] = -49, accompanied by the formation of CrF_3.

```
Conditions:
N=1, P=1E5, T=873, X(NI)=0.375136, X(CR)=4.7713E-2, X(MO)=5.4939E-2,
   X(LI)=0.1225, X(K)=0.1225, LNACR(F)=-41.5
DEGREES OF FREEDOM 0

Temperature    873.00 K (   599.85 C),  Pressure  1.000000E+05
Number of moles of components  1.00000E+00,  Mass in grams  3.57442E+01
Total Gibbs energy -2.34217E+05,  Enthalpy -1.79455E+05,  Volume  0.00000E+00

Component              Moles       W-Fraction  Activity   Potential  Ref.stat
CR                     4.7713E-02  6.9407E-02 6.8122E-23 -3.7048E+05 SER
F                      3.8814E-01  2.0630E-01 9.4794E-19 -3.0123E+05 GAS
FE                     3.1915E-13  4.9864E-13 0.000E+000 -2.5229E+15 SER
K                      1.2250E-01  1.3400E-01 1.7102E-21 -3.4709E+05 SER
LI                     1.2250E-01  2.3788E-02 1.0851E-22 -3.6710E+05 SER
MO                     4.0769E-02  1.0943E-01 2.8890E-04 -5.9153E+04 SER
NI                     2.7838E-01  4.5708E-01 1.2127E-02 -3.2027E+04 SER

FCC_A1                       Status ENTERED     Driving force  0.0000E+00
Moles 3.1915E-01, Mass 2.0249E+01, Volume fraction 0.0000E+00  Mass fractions:
NI  8.06841E-01  FE  8.80195E-13  K   0.00000E+00  F   0.00000E+00
MO  1.93159E-01  CR  8.19500E-13  LI  0.00000E+00

IONIC_LIQUID                 Status ENTERED     Driving force  0.0000E+00
Moles 4.9000E-01, Mass 1.0294E+01, Volume fraction 0.0000E+00  Mass fractions:
K   4.65256E-01  LI  8.25955E-02  MO  0.00000E+00  NI  0.00000E+00
F   4.52149E-01  CR  0.00000E+00  FE  0.00000E+00

CR1F3_S                      Status ENTERED     Driving force  0.0000E+00
Moles 1.9085E-01, Mass 5.2003E+00, Volume fraction 0.0000E+00  Mass fractions:
F   5.22934E-01  MO  0.00000E+00  K   0.00000E+00  NI  0.00000E+00
CR  4.77066E-01  LI  0.00000E+00  FE  0.00000E+00
```

Fig. 20. Hot corrosion of Alloy N under “aggressive” conditions, ln[ac(F)] = -41.5, accompanied by the formation of CrF_3.

Similar calculations conducted for Alloy 242 as shown in Figure 21 confirm the previous conclusion—it is more prone to hot corrosion, its onset taking place at "milder" conditions around ln[ac(F)] = -57.5 (i.e., practically 10 orders of magnitude weaker hot corrosion conditions than for Alloy N. The formation of a more oxidized CrF_3 also takes place in much milder conditions as shown in Figure 22.

Thus, we come to the conclusion that the 4-component simple representation of Alloy 242 and Alloy N was quite reasonable, and we confirm experimental results on the relative stability of these materials in molten salt.

As far as binary salt mixtures are concerned, Figure 22 below illustrates that hot corrosion for such system begins with the initial formation of $MoCl_4$, rather than chromium leaching process. These results will need to be verified experimentally in future research efforts.

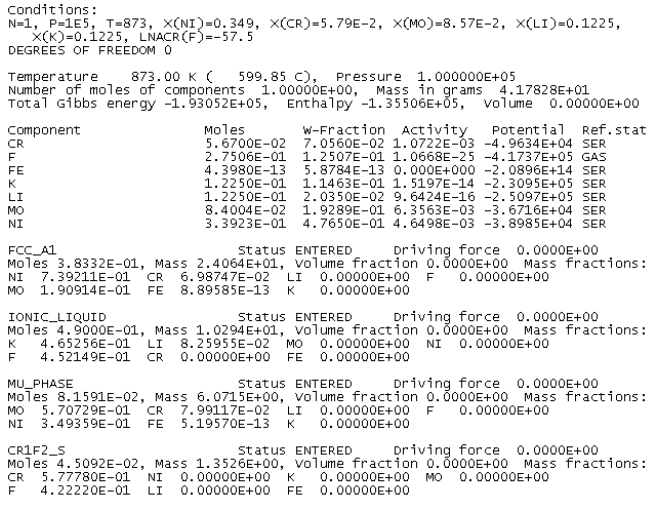

```
Conditions:
N=1, P=1E5, T=873, X(NI)=0.349, X(CR)=5.79E-2, X(MO)=8.57E-2, X(LI)=0.1225,
   X(K)=0.1225, LNACR(F)=-57.5
DEGREES OF FREEDOM 0

Temperature    873.00 K (   599.85 C),  Pressure  1.000000E+05
Number of moles of components  1.00000E+00,  Mass in grams  4.17828E+01
Total Gibbs energy -1.93052E+05,  Enthalpy -1.35506E+05,  Volume  0.00000E+00

Component               Moles       W-Fraction  Activity   Potential  Ref.stat
CR                      5.6700E-02  7.0560E-02 1.0722E-03 -4.9634E+04 SER
F                       2.7506E-01  1.2507E-01 1.0668E-25 -4.1737E+05 GAS
FE                      4.3980E-13  5.8784E-13 0.000E+000 -2.0896E+14 SER
K                       1.2250E-01  1.1463E-01 1.5197E-14 -2.3095E+05 SER
LI                      1.2250E-01  2.0350E-02 9.6424E-16 -2.5097E+05 SER
MO                      8.4004E-02  1.9289E-01 6.3563E-03 -3.6716E+04 SER
NI                      3.3923E-01  4.7650E-01 4.6498E-03 -3.8985E+04 SER

FCC_A1                       Status ENTERED     Driving force  0.0000E+00
Moles 3.8332E-01, Mass 2.4064E+01, Volume fraction 0.0000E+00  Mass fractions:
NI  7.39211E-01  CR  6.98747E-02  LI  0.00000E+00  F   0.00000E+00
MO  1.90914E-01  FE  8.89585E-13  K   0.00000E+00

IONIC_LIQUID                 Status ENTERED     Driving force  0.0000E+00
Moles 4.9000E-01, Mass 1.0294E+01, Volume fraction 0.0000E+00  Mass fractions:
K   4.65256E-01  LI  8.25955E-02  MO  0.00000E+00  NI  0.00000E+00
F   4.52149E-01  CR  0.00000E+00  FE  0.00000E+00

MU_PHASE                     Status ENTERED     Driving force  0.0000E+00
Moles 8.1591E-02, Mass 6.0715E+00, Volume fraction 0.0000E+00  Mass fractions:
MO  5.70729E-01  CR  7.99117E-02  LI  0.00000E+00  F   0.00000E+00
NI  3.49359E-01  FE  5.19570E-13  K   0.00000E+00

CR1F2_S                      Status ENTERED     Driving force  0.0000E+00
Moles 4.5092E-02, Mass 1.3526E+00, Volume fraction 0.0000E+00  Mass fractions:
CR  5.77780E-01  NI  0.00000E+00  K   0.00000E+00  MO  0.00000E+00
F   4.22220E-01  LI  0.00000E+00  FE  0.00000E+00
```

Fig. 21. Hot corrosion of Alloy 242 in "mild" conditions, ln[ac(F)] = -57.5, accompanied by the onset of formation of CrF_2.

Conditions:
N=1, P=1E5, T=873, X(NI)=0.349, X(CR)=5.79E-2, X(MO)=8.57E-2, X(LI)=0.1225,
X(K)=0.1225, LNACR(F)=-45.2
DEGREES OF FREEDOM 0

Temperature 873.00 K (599.85 C), Pressure 1.000000E+05
Number of moles of components 1.00000E+00, Mass in grams 3.49891E+01
Total Gibbs energy -2.45570E+05, Enthalpy -1.91218E+05, Volume 0.00000E+00

Component	Moles	W-Fraction	Activity	Potential	Ref.stat
CR	5.7900E-02	8.6043E-02	4.5077E-18	-2.8991E+05	SER
F	4.1870E-01	2.2735E-01	2.3436E-20	-3.2809E+05	GAS
FE	2.7840E-13	4.4437E-13	0.000E+000	-4.0751E+15	SER
K	1.2250E-01	1.3689E-01	6.9174E-20	-3.2023E+05	SER
LI	1.2250E-01	2.4301E-02	4.3890E-21	-3.4025E+05	SER
MO	5.4887E-02	1.5050E-01	8.3109E-04	-5.1483E+04	SER
NI	2.2352E-01	3.7492E-01	1.7697E-02	-2.9284E+04	SER

FCC_A1 Status ENTERED Driving force 0.0000E+00
Moles 2.7840E-01, Mass 1.8384E+01, Volume fraction 0.0000E+00 Mass fractions:
NI 7.13566E-01 FE 8.45734E-13 K 0.00000E+00 F 0.00000E+00
MO 2.86434E-01 CR 7.87416E-13 LI 0.00000E+00

IONIC_LIQUID Status ENTERED Driving force 0.0000E+00
Moles 4.9000E-01, Mass 1.0294E+01, Volume fraction 0.0000E+00 Mass fractions:
K 4.65256E-01 LI 8.25955E-02 MO 0.00000E+00 NI 0.00000E+00
F 4.52149E-01 CR 0.00000E+00 FE 0.00000E+00

CR1F3_S Status ENTERED Driving force 0.0000E+00
Moles 2.3160E-01, Mass 6.3106E+00, Volume fraction 0.0000E+00 Mass fractions:
F 5.22934E-01 MO 0.00000E+00 K 0.00000E+00 NI 0.00000E+00
CR 4.77066E-01 LI 0.00000E+00 FE 0.00000E+00

Fig. 22. Hot corrosion of Alloy 242 in "aggressive" conditions, ln[ac(F)] =-45.2, accompanied by the onset of formation of CrF_2.

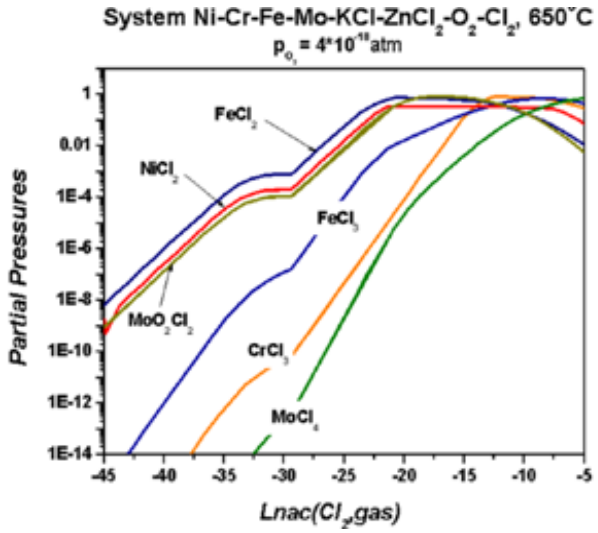

Fig. 23. Computational assessment of partial pressures of different hot corrosion products for the KCl-$ZnCl_2$ eutectic mixture and generic Ni-Cr-Fe-Mo alloy [33].

III. CONCLUSIONS

In this computational work, we modeled the behavior of Alloy 242 and Alloy N in a ternary molten salt eutectic mixture LiF-NaF-KF. It was established that the use of just four principal alloying elements—nickel, chromium, molybdenum, and iron—allows making quite reasonable conclusions about the nature of hot corrosion resistance of these materials. In turn, it probably implies that further alloy composition optimization work could be conducted to further enhance alloy hot corrosion resistance.

It was established, in complete agreement with earlier experimental studies that the onset of hot corrosion for both alloys is associated with chromium leaching and the formation of CrF_2 in relatively mild oxidizing conditions followed by the formation of CrF_3 in harsher conditions [9, 20]. However, for Alloy N the onset of hot corrosion takes place in much harsher conditions than for Alloy 242.

Significant deviations from these conclusions are not expected for binary molten salt mixture NaCl-$MgCl_2$; or in NaF-ZrF_4. However, thermodynamic data for these systems need to be generated in future research efforts in order to get a clearer picture of the mechanisms of hot corrosion onset.

In conclusion, continuing this computational research effort will allow nuclear engineers to approach the problem of down selection of materials for NGNP AHTRs with greater confidence, less effort spent on expensive experimental work, and in shorter periods of time.

ACKNOWLEDGMENTS

The authors are very grateful to Messrs. Ronald E. Mizia (INL, retired) and Denis E. Clark (INL, retired) for the initial support of their efforts in computational modeling of heterogeneous materials systems and experimental results that helped understanding and improving the obtained modeling results. Also, a special thank-you is extended to Mr. Michael W. "Mike" Patterson, MSNE, for his personal example and encouragement of one of the authors (MVG) in pursuing graduate studies in nuclear engineering.

The authors would like to thank Dr. David Holcombe, of the Oak Ridge National Laboratory, for reading portions of the manuscript and providing numerous recommendations, corrections, and suggestions for its improvement. Dr. Holcombe's insights helped the authors to see things in proper perspective and left them with a much better understanding of the enormity of the challenge of applying computational thermodynamics to the problem of hot corrosion of superalloys, - both for explaining well-established results and, particularly, providing meaningful advice to novel alloy developers.

Our research was supported by the Next Generation Nuclear Power Plant (NGNP) program (U.S. Department of Energy, Office of Nuclear Energy, Science, and Technology under DOE Idaho Operations Office Contract DE-AC0799ID13727; Manager –Mr. Michael W. "Mike" Patterson). This support is gratefully acknowledged, as well as that of the Center for Advanced Energy Studies for providing the necessary computational resources.

REFERENCES

1. P.SABHARWALL, H. SCHMUTZ, C. STOOTS AND G. GRIFFITH, "Tritium Permeation in High Temperature Reactors," *Proceedings of the ASME 2013 Summer Heat Transfer Conference*, 2013
2. P. SABHARWALL, E. S. KIM, M. MCKELLAR, N. ANDERSON, and M.W. PATTERSON, 2011, "Process Heat Exchanger Options for the Advanced High Temperature Reactor," INL/EXT-11-21584 (June 2011).
3. M.S. SOHAL P. SABHARWALL, P. CALDERONI, A. K. WERTSCHING, B. S. GROVER, and P. SHARPE, Conceptual Design of Forced Convection Molten Salt Heat Transfer Testing Loop, September 2010, External Report INL-10-19908 (September 2010)
4. D. BIELLO, "How to Use Solar Energy at Night," *Scientific American*, February 18, 2009.
5. S. PHOGIKAROON, "Molten Salt Technology," University of Idaho (January 2011).
6. D. A. SHORES and B. P. MOHANTY, "Role of Chlorides in High Temperature Corrosion of Fe-Cr-Ni Cast Alloy, Part II: Thermochemical Model Studies," *Corr. Sci.*, **46**, 2909 (2004).
7. D. A. SHORES, "New Perspectives on Hot Corrosion Mechanisms," *Proc. Intl. Conf. on High Temperature Corrosion*, Ed., R. A. Rapp, N. A. C. E. , Houston, p. 493 (1983).
8. M. V. GLAZOFF, A. TOKUHIRO, S.N.RASHKEEV, AND P. SABHARWALL, Zirconium, Zircaloy-2, and Zircaloy-4: Computational Thermodynamics and Atomistic Perspective on Hydrogen Uptake and Oxidation, ***Journal of Nuclear Materials***, vo.444, pp.65-75 (2014)
9. V. IGNATIEV, et al., "Compatibility of Selected Ni-based Alloys in Molten Li, Na, Be/F Salts with PuF3 and Tellurium Additions," *Nuclear Technology*, **164**, 130 (2008).
10. L. C. OLSON, "Materials Corrosion in Molten LiF-NaF-KF Eutectic Salt," Ph.D. Dissertation (Advisor – Prof. T. R. Allen) University of Wisconsin-Madison (2009).

11. D. F. WILLIAMS, L. M. TOTH, and K. T. CLARNO, "Assessment of Candidate Molten Salt Coolants for the Advanced High-Temperature Reactor (AHTR)," ORNL/TM-2006/12, Oak Ridge National Laboratory (2006).
12. P. CHARTRAND, and A. D. PELTON, "Thermodynamic Evaluation and Optimization of the LiF-NaF-KF-MgF_2-CaF_2 System Using the Modified Quasi-Chemical Model," *Metallurgical and Materials Transactions A*, **32A**, 6, 1385–1396 (2001).
13. FACTSTAGE, "FSalt Thermodynamic Database for Molten Salt Applications" (2011).
14. M. HILLERT, "Phase Equilibria, Phase Diagrams, and Phase Transformations; Their Thermodynamic Basis," 2nd Edition, Cambridge University Press, Cambridge, UK (2008).
15. HAYNES INTERNATIONAL, "Haynes 242 Alloy, Technical Description," Kokomo, Ind., publication H-3079E (2000).
16. M. K. MILLER, I. M. ANDERSON, L. M. PIKE, and D. L. KLARSTROM, "Coherent Ni2(Cr, Mo) Precipitates in Ni-21Cr-17Mo Superalloy," *Mat. Sci. and Eng.* A, **327**, 1, 89–93 (2002).
17. H. L. LUKAS, S. G. FRIES, and B. SUNDMAN, "Computational Thermodynamics, The CALPHAD Method," Cambridge University Press, Cambridge, UK (2007).
18. H. E. MCCOY, Jr., 1971, "An Evaluation Of The Molten-Salt Reactor Experiment Hastelloy N Surveillance Specimens - Fourth Group," ORNL/TM-3063 (March 1971).
19. J. W. KOGER, and A. P. LITMAN, "Mass Transfer between Hastelloy N and Haynes Alloy 25 in a Molten Sodium Fluroborate Mixture," ORNL-'I'M-3488 (October 1971).
20. P., SHI, A. ENGSTROM, and B. SUNDMAN, 2008, "ThermoCalc Calculations for Materials in Corrosive Environments," *SINTEF Symposium,* Trondheim, Norway (May 2008).
21. R.W. CAHN, The Coming of Materials Science, Pergamon, Amsterdam (2001).

22. Z.-K. LIU, First-Principles calculations and CALPHAD Modeling of Thermodynamics, Journal of Phase equilibria and Diffusion, published online 03 September (2009).
23. N. SAUNDRES and A.P. MIODOWNIK, CALPHAD – Calculation of Phase Diagrams. A Comprehensive Guide, Pergamon, London (1998).
24. DICTRA Version 25 User's Guide, 2010, Thermo-Calc Software AB, Stockholm, Sweden.
25. ThermoCalc Classic Version S User's Guide, P. Shi and B. Sundman Editors, ThermoCalc Software AB, Stockholm, Sweden (2010).
26. O. BENES, Thermodynamics of Molten Salts for Nuclear Applications, Ph.D. Dissertation, Advisors: Dr. David Sedmidubský, and Dr. Rudy J. M. Konings, Prague (2008).
27. G. HATEM, F. TABARIES, and F. GAUNE-ESCARD, Enthalpies de formation des melanges liquides ZrF_4-MF (M = Li, Na, K, Rb), *Thermochimica Acta,* vol. 149, pp.15-26 (1989)
28. H. E. McCOY, Jr., Status of Materials Development for Molten Salt Reactors, ORNL/TM-5920 (January 1978)
29. R.E. THOMA and W.R. GRIMES, Phase Equilibrium Diagrams For Fused Salt Systems, ORNL Chemistry Division, Technical Report # W-7485-eng-26, June 24 1957. Based on: ANI Quarterly Progress Report June 10, 1952, ORNL-1294, p.91
30. R.E. THOMA (Editor), Phase Diagrams of Nuclear Reactor Materials, Oak Ridge National Laboratory, ORNL-2542, November 20, 1959.
31. M.V. GLAZOFF, Thermodynamic Assessment of Hot Corrosion Mechanisms of Superalloys Hastelloy N and Haynes 242 in Eutectic Mixture of Molten Salts KF and ZrF_4, INL External Report INL/EXT-12-24617 (revision 1, September 28, 2012)

32. V. DRACOPOULOS, J. VAGELATOS and G. N. PAPATHEODOROU, Raman spectroscopic studies of molten ZrF_4–KF mixtures and of A_2ZrF_6, A_3ZrF_7 (A = Li, K or Cs*)* compounds *J. of Chemical Society, Dalton Transactions*, issue 7, pp.1117-1122 (2001).

33. F. J. P. TRUJILLO, "Surface Engineering and Nanostructured Materials," UCM 910627, Madrid, Spain (2011).